Draft version February 5, 2008
Preprint typeset using LaTeX style emulateapj v. 11/12/01

INFRARED DARK CLOUDS: PRECURSORS TO STAR CLUSTERS

J. M. Rathborne and J. M. Jackson
Institute for Astrophysical Research, Boston University, Boston, MA 02215; rathborn@bu.edu, jackson@bu.edu
AND

R. Simon
I.Physikalisches Institut, Universität zu Köln, 50937 Köln, Germany; simonr@ph1.uni-koeln.de
Draft version February 5, 2008

ABSTRACT

Infrared Dark Clouds (IRDCs) are dense molecular clouds seen as extinction features against the bright mid-infrared Galactic background. Millimeter continuum maps toward 38 IRDCs reveal extended cold dust emission to be associated with each of the IRDCs. IRDCs range in morphology from filamentary to compact and have masses of 120 to 16,000 $M_{\odot}$, with a median mass of $\sim$940 $M_{\odot}$. Each IRDC contains at least one compact ($\leq$0.5 pc) dust core and most show multiple cores. We find 140 cold millimeter cores unassociated with *MSX* 8 μm emission. The core masses range from 10 to 2,100 $M_{\odot}$, with a median mass of $\sim$120 $M_{\odot}$. The slope of the IRDC core mass spectrum ($\alpha \sim 2.1 \pm 0.4$) is similar to that of the stellar IMF. Assuming that each core will form a single star, the majority of the cores will form OB stars. IRDC cores have similar sizes, masses, and densities as hot cores associated with individual, young high-mass stars, but they are much colder. We therefore suggest that IRDC represent an earlier evolutionary phase in high-mass star formation. In addition, because IRDCs contain many compact cores, and have the same sizes and masses as molecular clumps associated with young clusters, we suggest that IRDCs are the cold precursors to star clusters. Indeed, an estimate of the star formation rate within molecular clumps with similar properties to IRDCs ($\sim 2\ M_{\odot}\,\mathrm{yr}^{-1}$) is comparable to the global star formation rate in the Galaxy, supporting the idea that all stars may form in such clumps.

Subject headings: ISM: clouds–dust, extinction–stars: formation

1. INTRODUCTION

Although high-mass stars (>6 $M_{\odot}$) have a profound effect on the Galactic environment and are responsible for recycling and enriching interstellar matter, their early evolutionary phases are not well known. Because they evolve rapidly, high-mass stars have a short lifetime. In addition, high-mass stars emit copious amounts of UV photons, which quickly heat, ionize, and disrupt their natal molecular clouds. Thus, direct observations of their earliest stages are difficult.

Because high-mass stars invariably form in star clusters, to understand high-mass star formation it is important to study the earliest stages in the formation of star clusters. Molecular line, infrared (IR), and millimeter continuum studies of young, embedded clusters show that star clusters form from small ($\sim$0.5–1 pc), massive ($\sim$100–1000 $M_{\odot}$), and dense ($\sim 10^4$–$10^6\,\mathrm{cm}^{-3}$) molecular clumps within a giant molecular cloud (see Table 1; Lada & Lada 2003; Motte et al. 2003). Cluster-forming clumps have star-formation efficiencies of $\sim$ 10–30% and a highly fragmented sub-structure (Lada et al. 1997). Within these clumps, the densest, most compact sub-structures, called "cores", give rise to individual stars.

The emerging picture of star formation begins with the fragmentation of a molecular cloud (e.g. Shu et al. 1987). Observational evidence suggests that molecular clouds are fragmented on all size scales (Williams et al. 2000). The cloud eventually condenses into cold, gravitationally bound starless cores. As the core becomes centrally concentrated and begins to collapse gravitationally, a protostar and disk system is formed as material is accreted from its surroundings. Soon thereafter, bipolar outflows and jets are formed as a consequence of the accretion process. The central star then emerges from the molecular cloud to be an optically visible main-sequence star.

For low-mass stars, the theory is well developed (e.g. Shu 1991), and all of these evolutionary stages are observed (e.g. Lada 1999). The earliest stage in the formation of low-mass stars are identified as Bok globules. These are isolated, well-defined patches of optical obscuration (A_v=1–25 mag) viewed against background stars (Bok & Reilly 1947). Because of their isolation and uncomplicated environments, Bok globules have been studied extensively and have provided an excellent observational perspective of the initial conditions within low-mass star-forming molecular clouds. Many studies of Bok globules have used optical and IR star counts to trace their visual extinctions and, hence, have measured their column densities, masses, and internal structure (e.g. Lada et al. 1994; Alves et al. 2001; Lombardi & Alves 2001). Bok globules have small sizes (0.1–2 pc), characteristic masses of 1–100 $M_{\odot}$, and a simple morphology (see Table 1; Leung 1985; Clemens & Barvainis 1988; Bourke et al. 1995).

Within Bok globules, the dense, compact pre-cursors to the individual protostars are found. These so-called "pre-protostellar cores" have low temperatures ($\sim$ 10 K), compact sizes ($\sim$0.05 pc), low masses (0.5–5 $M_{\odot}$), and high densities (10^5–10^6 cm^{-3}; see Table 1; e.g. Myers & Benson 1983; Ward-Thompson et al. 1994). Once the embedded protostar begins to evolve toward the main-sequence,

it emits strongly in the IR (e.g. Lada & Wilking 1984; Adams et al. 1987) and reveals molecular outflows, jets, and Herbig-Haro objects (e.g. Snell et al. 1980; Bally & Lada 1983; Fukui et al. 1993).

In contrast, the early evolution of high-mass stars is not as well understood. Observationally, the earliest known, well-characterized phase of high-mass star formation is associated with a special class of molecular cores called "hot cores." Hot cores are internally heated (50–250 K), small (<0.1 pc), massive (∼100–300 $M_{\odot}$), and dense (10^5–$10^8\,\mathrm{cm}^{-3}$; see Table 1; Garay & Lizano 1999; Kurtz et al. 2000; Churchwell 2002). In the later stage of the hot core phase, molecular outflows and maser emission appear, both of which are signatures of an accretion disk (Garay & Lizano 1999; Kurtz et al. 2000). This stage marks the appearance of ultra-compact H II regions, the small, dense regions of ionized gas which surround the embedded high-mass main-sequence star.

These observed early evolutionary stages of high-mass stars represent a phase *after* the central protostar has already formed. A complete understanding of the formation of high-mass stars, however, must begin with an earlier phase, before the formation of the protostar. Presumably, high-mass stars will also proceed through stages analogous to the Bok globules and pre-protostellar cores found in the case of low-mass star formation. So far, however, observational examples of these phases for high-mass stars have remained elusive.

By analogy, we expect the high-mass equivalents of Bok globules and high-mass starless cores also to be cold. However, because they are the precursors to high-mass stars, they should have larger sizes, masses, column densities, and volume densities. Because the high-mass Bok globule analogs are likely to be cold and very dense, one might expect to detect them as extinction features and to trace their internal structure through millimeter/submillimeter continuum imaging.

We suggest that the earliest stage of high-mass star formation occurs within infrared dark clouds (IRDCs). IRDCs are defined as regions of high extinction viewed against the bright, diffuse mid-IR Galactic background. IRDCs, first detected by *ISO* and then by *MSX* (Perault et al. 1996; Egan et al. 1998; Hennebelle et al. 2001), are ubiquitous throughout the Galaxy (Simon et al. 2006a). Previous studies show that their molecular material has low temperatures (< 25K), high column densities (∼ 10^{23}–$10^{25}\,\mathrm{cm}^{-2}$), and high volume densities (>10^5 cm^{-3}; Egan et al. 1998; Carey et al. 1998, 2000). A recent molecular line study of a large sample of IRDCs establishes their kinematic distances and shows that their Galactic distribution is enhanced towards the Galaxy's most massive star forming structure, the so-called 5 kpc ring (Simon et al. 2006b). Millimeter/submillimeter studies of a few IRDCs show that they harbor compact cores (Lis & Carlstrom 1994; Carey et al. 2000; Redman et al. 2003; Garay et al. 2004; Ormel et al. 2005; Rathborne et al. 2005).

We have developed an algorithm (Simon et al. 2006a) to identify IRDCs as regions within the *MSX* 8 μm Galactic Plane Survey (Price et al. 2001) that have a significant decremental contrast[1] against a modelled background. IRDCs were identified from contrast images if they met two conditions; (1) they must be regions of contiguous pixels whose measured contrast lies at least 2σ above the instrumental noise, and (2) they must have solid angles > 1,200 square arcsec. Because the Galactic background is highly variable, the signal-to-noise, and hence the significance level, is non-uniform for this sample. Simon et al. (2006a) find 10,961 IRDCs meeting these criteria[2].

Because IRDCs are extinction features seen against the Galactic mid-IR background, their identification is strongly biased toward nearby clouds and clouds that lie in front of bright mid-IR background emission. Almost certainly, clouds with identical temperatures, sizes, masses, column densities, and volume densities as known IRDCs have escaped detection. These undetected clouds will preferentially lie on the far side of the Galaxy, behind the bulk of the Galaxy's diffuse mid-IR emission, or in the outer Galaxy, where the Galactic mid-IR background is faint.

Because IRDCs are cold, their thermal dust emission peaks at millimeter/submillimeter wavelengths. Consequently, we can best study their internal structure by imaging at these wavelengths. A further advantage is that the dust emission at millimeter wavelengths is optically thin. Thus, unlike optically thick molecular line emission, the millimeter dust continuum is a more accurate tracer of column density and mass.

In this paper, we show that IRDCs are cold molecular clumps with sizes and masses identical to those of the warmer cluster-forming clumps. Moreover, we find that IRDCs contain compact cores with sizes, masses, and densities comparable to high-mass star-forming hot cores, the only obvious difference being that IRDC cores are colder. We therefore suggest that IRDCs are the cluster-forming, high-mass analogs to Bok globules, and their embedded cores the precursors to individual high-mass protostars.

2. OBSERVATIONS

For this study, we selected the 38 darkest IRDCs with known kinematic distances from the sample of Simon et al. (2006b). The local standard of rest (LSR) velocity for each IRDC was determined from a morphological match of the mid-IR extinction to ^{13}CO emission from the Boston University–Five College Radio Astronomy Observatory Galactic Ring Survey (Simon et al. 2001; Jackson et al. 2006). Velocities were converted to a Galactocentric radius and kinematic distance using the Clemens (1985) rotation curve[3] scaled to R_0=8.5 kpc and Θ_0=220 $\mathrm{km\,s}^{-1}$. Because IRDCs are extinction features, they are assumed to lie at the near kinematic distance. The IRDCs within our sample show the highest peak contrast relative to the extended mid-IR background (> 36%) and span a broad range in distance and Galactic location.

The 1.2 mm continuum data toward the IRDCs were ob-

[1] Defined as contrast=(background-image)/background.

[2] IRDCs from this catalog are called "MSXDC G" followed by their Galactic coordinates. For simplicity we will drop the "MSXDC" labels in the text.

[3] For the portion of the Galaxy sampled, the use of the more recent Brand & Blitz (1993) rotation curve does not significantly alter the derived distances and therefore will not affect any of our conclusions.

tained at the Institut de Radioastronomie Millimétrique (IRAM) 30 m telescope using the 117 element bolometer array MAMBO II in 2003 December and 2004 January–March. The FWHM angular resolution of each element in the array is 11″. The angular separation between array elements is 20″. Because the morphology of the IRDCs ranged from compact to filamentary, we mapped each of the IRDCs using the on-the-fly mapping mode with a size large enough to cover the extent of the mid-IR extinction. The map sizes ranged from $3' \times 3'$ to $9' \times 9'$. The scanning speed was 6 arcsec s^{-1} for maps $6' \times 6'$ or smaller, and 8 arcsec s^{-1} for larger maps. To sample the emission fully, all maps were obtained in the 'sweeping' mode, where the spacing between sub-scans was set to 22″. Pointing and sky-dip calibrations were performed regularly.

All data reduction was achieved within the MOPSI package[4]. All maps were reduced by applying the atmospheric opacity corrections, fitting and subtracting a baseline, and removing the correlated sky noise. Maps were flux calibrated using the conversion factor obtained from the counts detected in observations of Uranus. The rms noise level in each of the final maps is ~ 10 mJy beam^{-1}.

3. RESULTS

3.1. *Global Millimeter Emission Characteristics*

Millimeter continuum emission was detected toward all 38 of the IRDCs observed. Figures 1–6 show the 1.2 mm continuum emission toward each IRDC overlaid on the *MSX* 8 μm image. In all cases, the morphology of the millimeter continuum emission matches the mid-IR extinction extremely well.In addition, all IRDCs have at least one bright, compact millimeter source; most show multiple, compact sources superimposed on fainter, extended emission.

Although IRDCs all exhibit extinction in the mid-IR, their morphologies vary considerably. Their shapes can be simple and unstructured on the one hand, and complex and filamentary on the other. For example, the IRDCs G028.08+00.07 (Fig. 3[c]) and G035.59-00.24 (Fig. 5[e]) show little sub-structure, whereas G034.43+00.24 (Fig. 5[b]) and G035.39−00.33 (Fig. 5[d]) are highly filamentary. Some IRDCs also show a complicated internal sub-structure with 10 or more compact cores, for example, G024.33+00.11 (Fig. 2[c]), G028.37+00.07 (Fig. 3[f]), G028.53−00.25 (Fig. 4[a]), and G033.69−00.01 (Fig. 5[a]).

By eye we have catergorized each IRDC as either "compact" or "filamentary" based on the morphology of the millimeter continuum emission. We find 22 IRDCs are compact, while 16 are filamentary. We find a slight trend for higher mass cores to be found within the filamentary clouds. For compact IRDCs the average mass of the most massive core is $\sim 210\ M_\odot$. For filamentary IRDCs, however, the average mass of the most massive core is $\sim 660\ M_\odot$, about a factor of 3 higher.

The degree to which IRDCs are associated with mid-IR continuum emission sources is highly variable. For example, G015.31−00.16 (Fig. 1[b]), G022.73+00.11 (Fig. 1[f]), and G024.60+00.08 (Fig. 2[d]) show no obvious association with any mid-IR continuum emission source in *MSX* 8 μm images (to a sensitivity limit of 1.3 MJy sr^{-1}; Price et al. 2001). On the other hand, G028.28−00.34 (Fig. 3[e]) and G053.11+00.05 (Fig. 6[c]) appear to be associated with very bright, resolved mid-IR emission sources. There is no obvious correlation between the presence of a bright mid-IR emission source with any millimeter continuum observational characteristic of the IRDC.

3.2. *IRDC Masses*

Reliable mass estimates of IRDCs using molecular lines are problematic because the lines are often highly opaque and thus do not trace their embedded interiors. In addition, because IRDCs are so cold, molecules are frozen onto dust grains in their centers. Because dust is optically thin and not depleted, it is a better mass tracer. We use the 1.2 mm continuum emission to estimate the cloud mass using the expression

$$M = \frac{F_\nu D^2}{\kappa_\nu B_\nu(T)} \quad (1)$$

(Hildebrand 1983), where F_ν is the observed integrated source flux density, D is the distance, κ_ν is the dust opacity per gram of dust, and $B_\nu(T)$ is the Planck function at the dust temperature. We adopt for $\kappa_{1.2mm}$ a value of 1.0 cm^2 g^{-1} (Ossenkopf & Henning 1994) and assume a gas-to-dust mass ratio of 100. We assume graybody emission with an emissivity index β of 2 (Carey et al. 2000; Rathborne et al. 2005). We also assume a dust temperature of 15 K, which is consistent with temperature estimates from molecular line emission (Teyssier et al. 2002), previous observations of a few IRDCs at submillimeter wavelengths (Carey et al. 2000), and the fact that some IRDCs are seen as extinction features up to 100 μm (Egan et al. 1998).

The derived masses will be underestimated if the value for β is lower than the assumed value of 2 (e.g., β of 1 will increase the IRDC masses by about 10%) and overestimated if the temperature is higher than the assumed value of 15 K (e.g., a dust temperature of 30 K will reduce the IRDC masses by $\sim$ 40%). The derived masses are proportional to the assumed value of κ_ν.

Table 2 lists, in order of increasing Galactic longitude, each of the IRDCs, the coordinates of the peak contrast (Simon et al. 2006a), the LSR velocity (V_{LSR}), line width (ΔV) and kinematic distance (D; Simon et al. 2006b), the peak and integrated 1.2 mm flux, and the mass. The integrated 1.2 mm fluxes were obtained by summing the 1.2 mm continuum emission above a 3σ level (>30 mJy beam^{-1}) over the extent of the mid-IR extinction feature. The total mass of the IRDCs were calculated using the integrated flux and were found to range from 120 to 16,000 $M_\odot$, with a median mass of 940 $M_\odot$ and an average mass of $\sim$ 3,000 $M_\odot$. Figures 1–6 show that the millimeter emission associated with each IRDC typically extends a few arcmins, or a few parsecs given their distances.

3.3. *Compact Cores*

Compact cores were identified by fitting two-dimensional gaussians to the peaks (>8σ) within the 1.2 mm continuum images. Each Gaussian was subtracted before the next was fit until the image contained only extended emission. The number of cores found within each

[4] MOPSI was developed by Robert Zylka.

IRDC ranged from 1 to 18. Toward the 38 IRDCs, we detected a total of 188 compact cores, increasing the sample of known cores within IRDCs from ∼10 (Carey et al. 2000; Redman et al. 2003; Garay et al. 2004).

Table 3 lists the properties of the cores, including: their designation, coordinates, peak and integrated 1.2 mm flux, average angular and physical sizes, and mass. The cores are named in order of decreasing peak 1.2 mm flux with the designation "MM" (e.g., MM1, MM2, etc). Because the 1.2 mm images extend beyond the IRDC, they often include nearby, bright millimeter cores that are associated with strong 8 μm emission sources (and in some cases IRAS sources). We find 48 of the cores are associated with *MSX* 8 μm emission. These "warm" cores are included within our list, but are marked as being associated with 8 μm emission and not an extinction feature (an "em" in the comment column of Table 3). These cores are not included in the following analyses. Thus, removing these "warm" cores from our sample, we find 140 "cold" millimeter cores associated with the 38 IRDCs.

Masses for these compact 1.2 mm cores were calculated from the integrated flux from the two-dimensional Gaussian fit to the core. A histogram of the derived masses for the "cold" compact cores is shown in Figure 7. These cores range in mass from 10 to 2100 $M_{\odot}$, with a median value of 120 $M_{\odot}$. We find that 67% of our sample lies in the mass range 30 to 300 $M_{\odot}$. For masses >100 $M_{\odot}$ the distribution is roughly a power law with an index α (dN/dM $\sim$ M$^{-\alpha}$) of 2.1 $\pm$ 0.4. The apparent peak near M∼45 $M_{\odot}$ reflects our completeness limit. Because the cores lie at different distances, the mass detection limit varies from cloud to cloud. At the median distance of our sample of ∼4.0 kpc, the 8σ core detection limit corresponds to a mass of ∼30 $M_{\odot}$. Hence, below ∼ 45 $M_{\odot}$, our "cold" core sample is incomplete.

For three active star-forming cores within G034.43+00.24, Rathborne et al. (2005) find that greybody fits to their IR to millimeter continuum spectral energy distributions reveal temperatures of ∼ 30K. Thus, these masses will be overestimates if any of the cores have a higher temperature than 15 K (e.g., a dust temperature of 30 K will reduce the core mass by ∼ 40%).

The cores have diameters in the range 0.04 to 1.6 pc, with a median diameter of 0.5 pc. All cores are resolved in the 11″ IRAM beam. Figure 8 plots the size versus mass for the millimeter cores. The majority of cores have masses <200 $M_{\odot}$ and sizes <0.8 pc. We find no correlation between either the mass or size and kinematic distance (Fig. 9). Indeed, we detect low-mass cores at all distances.

Figure 10 plots the histogram of the core densities. The densities were calculated using

$$\rho = \frac{3M}{4\pi r^3} \quad (2)$$

where M is the 1.2 mm mass and r is the radius (half the size given in Table 3). The densities range from 10^3 to 10^7 cm^{-3}, with a median value of 3.3×10^4 cm^{-3}.

4. DISCUSSION

The combination of low optical depth and good angular resolution of these millimeter images allow us to probe the internal structure of IRDCs and to elucidate their role in the star formation process.

The sizes and masses of IRDCs as a whole are larger than those of Bok globules and hot cores, but smaller than those of giant molecular clouds. Instead, IRDCs more closely resemble cluster-forming molecular clumps. Indeed, IRDC sizes (∼ 2 pc) and masses (∼10^2–10^4 $M_{\odot}$) are comparable to those of cluster-forming clumps (see Table 1). Moreover they both exhibit a highly fragmented sub-structure. A significant difference, however, is that IRDCs are much colder.

4.1. *A Proposed Evolutionary Sequence for IRDCs*

Because the masses and sizes of IRDCs and cluster forming clumps are so similar, we suggest that IRDCs are the high-mass analogs to Bok globules. As such, they are the precursors to star clusters. Their lower temperatures would then result purely from an evolutionary effect. IRDCs may be colder because they represent an early stage of a cluster-forming molecular clump before the stars have formed and heated the surrounding gas and dust.

If this scenario is correct, clusters begin their lives as cold, pristine IRDCs (in this discussion, we will refer to *all* molecular clumps with similar temperatures [∼ 15 K], sizes [∼ 2 pc], masses [∼10^2–10^4 $M_{\odot}$], and densities [∼10^2–10^4 cm^{-3}] as the *MSX* dark clouds as "IRDCs", whether or not they are actually observed as extinction features). As cores begin to collapse within the clump, protostars form and begin to heat their local environment. If high-mass protostars are present, they eventually will form zero-age main-sequence OB stars which will rapidly heat, ionize, and disrupt their surroundings.

We thus expect an evolutionary sequence for IRDCs as follows. The youngest IRDCs will be isolated IR dark clouds, unassociated with any bright, extended mid-IR or radio continuum emission. As protostars form, the IRDC cores will be bright, compact far-IR sources but the IRDC itself will remain dark. In the later stages, the IRDC will have formed OB stars which will illuminate and ionize significant portions of the cloud. Such IRDCs will contain very bright, extended mid-IR emission and compact H II regions. Eventually, the IRDC will lose its 'darkness' and become an IR bright star forming region.

We suggest that the degree to which IRDCs are associated with mid-IR continuum emission sources is precisely due to this evolutionary sequence. IRDCs with no associated mid-IR emission sources such as G015.31−00.16 (Fig. 1[a]) and G028.53−00.25 (Fig. 4[a]) represent the very earliest stage before high-mass protostars have formed. The intermediate stage might be represented by G034.43+00.24 (Fig. 5[b]). Rathborne et al. (2005) demonstrate that this IRDC is the site of recent, active high-mass star formation. Examples of the later evolutionary stage are G028.28−00.34 (Fig. 3[e]) and G053.11+00.05 (Fig. 6[c]). Toward both of these IRDCs we see bright, extended mid-IR emission. These bright sources appear to be H II regions breaking out of the dense cloud.

4.2. *IRDC Cores: Precursors to Hot Cores*

Whereas cluster formation takes place over size scales of several parsecs and involves ∼10^3 $M_{\odot}$ of molecular gas, individual stars form from smaller, less massive sub-

structures. Individual low-mass stars form within Bok globules from pre-protostellar cores with characteristic sizes of ∼0.05 pc, masses of 0.5–5 $M_\odot$, and densities of $\sim 10^5$–$10^6 \mathrm{cm}^{-3}$ (see Table 1). High-mass stars should form from similar cold, compact cores, but with higher masses and densities. However, the earliest well characterized stage of high-mass star formation is the hot core phase, well after the formation of the central protostar.

Just as IRDCs have similar sizes and masses compared to cluster-forming clumps, the IRDC cores also share some of the properties of hot cores that are associated with individual high-mass stars. Both the IRDC cores (∼ 0.3 pc) and hot cores (< 0.1 pc) are compact. In our sample, IRDC cores have a median mass of 120 $M_\odot$. We find that 67% have masses in the range 30–300 $M_\odot$ (see Fig. 7), which is comparable to the measured mass for hot cores ∼ 100–300 $M_\odot$ (Garay & Lizano 1999). Their densities are also comparable; IRDC cores in our sample range from 10^3–$10^7\,\mathrm{cm}^{-3}$ while hot cores, have slightly larger densities ranging from 10^5–$10^8\,\mathrm{cm}^{-3}$ (see Table 1).

These similarities suggest that IRDC cores may be the cold precursors to hot cores and the high-mass analogs of pre-protostellar cores within Bok globules. If true, then hot cores collapse from IRDC cores, and therefore we should expect the IRDC cores to be somewhat larger and less dense. Indeed, the observations show that the IRDC cores are factors of several larger and factors of ∼ 30 less dense than hot cores.

The mass of the star that forms within an IRDC core depends on fragmentation and the molecular core's star formation efficiency. In the simplest scenario, a single core forms a single star. Unfortunately, the core star formation efficiency is not well known. Lada et al. (1997) find efficiencies ranging from 10-30% in cluster-forming clumps. If we adopt a value of ∼ 20% as a typical core star formation efficiency, the majority of our cores will form stars with masses ranging from 6 to 60 $M_\odot$ corresponding to OB stars. We conclude therefore that IRDC cores are the precursors to high-mass protostars. In fact, Rathborne et al. (2005) find three high-mass protostars associated with IRDC cores in G034.43+00.24.

We cannot yet exclude, however, the possibility that some IRDC cores may instead further fragment to form several low- to intermediate-mass stars. Indeed, the most massive (>500 $M_\odot$) cores with compact (<0.5 pc) sizes will likely further fragment into several protostellar objects. Because the central protostar is directly revealed by its millimeter through mid-IR emission, the number of detected millimeter to mid-IR sources within these cores will trace the degree of fragmentation, and more importantly, reveal the luminosities of the individual protostars. Thus, higher angular resolution studies, in the millimeter/submillimeter and mid-IR, are necessary to distinguish between single and multiple protostars. In addition, such observations would also reveal the luminosities and, hence, masses of the individual protostars.

Because high-mass IRDC cores are brighter at millimeter wavelengths than low-mass cores, the lack of detected low-mass cores may result from our limited sensitivity. Because the number of cores as a function of mass N(M) is well characterized by a power law for masses >100 $M_\odot$, one might expect the number of low-mass cores to follow this trend. It is possible therefore that low-mass cores exist in large numbers within IRDCs but are simply fainter than our detection limit. Toward the nearby clouds, we do detect a few low-mass cores (∼10 $M_\odot$); it is likely these will only give rise to low-mass stars.

4.3. *Implications for the Role of IRDCs in Galactic Star Formation*

The discovery of a large number of IRDCs and cores has important implications for their role in global star formation in the Galaxy. If IRDCs spawn star clusters, and stars form predominantly in clusters (Lada & Lada 2003), then every star in the Galaxy may very well form within molecular clumps with identical temperatures, sizes, masses, column densities, and volume densities as IRDCs. These clumps would only appear as an IRDC if they happened to be nearby, with a strong mid-IR background.

A very rough estimate of the star formation rate within IRDC-like molecular clumps can be made as follows. The total mass in the form of IRDCs, $M_{IRDC,tot}$, can be estimated using

$$M_{IRDC,tot} = N_{IRDC} < M_{IRDC} > \frac{1}{f_{detect}} \qquad (3)$$

where N_{IRDC} is the total number of known IRDCs in the Galaxy, $< M_{IRDC} >$ is the characteristic mass of an individual IRDC, and f_{detect} is the fraction of all IRDCs that can be detected as extinction features. Although our sample comes from the *MSX* database, new and future surveys will no doubt improve our understanding of IRDCs due to improved sensitivity and angular resolution. For example, the *Spitzer* 3–8 μm Galactic Legacy Infrared Mid-Plane Survey Extraordinaire (GLIMPSE; Benjamin et al. 2003), improves the angular resolution by an order of magnitude over *MSX* and therefore reveals new IRDCs. *MSX*, however, does detect the largest, most massive IRDCs that presumably dominate Galactic star-formation.

From the *MSX* database, roughly 10,000 IRDCs have been identified (Simon et al. 2006a). If the IRDCs in our sample are typical, then we can choose their average mass as a characteristic mass for IRDCs, and so $< M_{IRDC} > \sim$ 3,000 $M_\odot$. The total number of IRDCs in the Galaxy is not yet known. Because of strong observational bias only a fraction, f_{detect}, of all IRDCs are actually detected as extinction features. Toward the inner Galaxy, IRDCs at the far kinematic distance will lie behind most of the diffuse IR emission and would be impossible to detect as extinction features. From geometrical arguments, sources within the solar circle at the near kinematic distance occupy 1/3 of the area of sources at the far kinematic distance. Since we preferentially detect IRDCs at the near kinematic distance we estimate $f_{detect} \sim 1/3$. With these estimates, the total Galactic mass contained in IRDCs is $\sim 10^8$ $M_\odot$, or about 5% of the total molecular gas content of the Milky Way.

The rate of star formation $\dot{M}$ occurring within IRDCs can now be estimated using

$$\dot{M}_{SF} = \frac{\eta M_{IRDC,tot}}{\tau_{SF}} \qquad (4)$$

where η is the star formation efficiency, and τ_{SF} is the timescale for star formation to occur within an IRDC. If

we choose an efficiency of $\eta \sim 0.2$ (typical for cluster forming clumps) and a conservative star formation timescale of 10^7 yr, we arrive at a total star formation within IRDCs of $\dot{M} \sim 2\ M_\odot\ \mathrm{yr}^{-1}$. This star formation rate is quite close to estimates of the global star formation of the Galaxy, $\sim$ 3–5 $M_\odot\ \mathrm{yr}^{-1}$ (Prantzos & Aubert 1995). While this estimate is only approximate, it does support the plausibility of the idea that IRDC-like molecular clumps are the birthplaces of all stars.

4.4. *Comparison to the Stellar IMF*

If stars form within IRDC cores, then it is also interesting to compare the mass spectrum of IRDC cores with the stellar initial mass function (IMF). If these high-mass cores spawn single high-mass stars with a constant star formation efficiency, one might expect the power law index α to match that of the IMF for high-mass stars. Indeed, recent studies suggest that the stellar initial mass function is determined by the fragmentation of a cloud into cores, well before any stars have formed (Motte et al. 1998; Testi & Sargent 1998; Blitz & Williams 1999; Williams et al. 2000; Churchwell 2002).

Above $M \sim 100\,M_\odot$, we find the IRDC core mass spectrum is approximately a power law with an index α of 2.1 ± 0.4. Within the errors, this power-law index is the same as that for the stellar IMF for high-mass stars ($\alpha \sim 2.35$; Salpeter 1955) and also to that of the clump mass spectrum for molecular clouds ($\alpha \sim 1.8$; Kramer et al. 1998; Simon et al. 2001).

5. CONCLUSIONS

We used MAMBO II on the IRAM 30 m telescope to image the 1.2 mm continuum emission toward a sample of 38 IRDCs with known kinematic distance. We find 1.2 mm continuum emission to be associated with each of the IRDCs observed. The morphology of the 1.2 mm continuum emission matches the mid-IR extinction features extremely well; some IRDCs are extended and filamentary, while others are compact and smooth. Every IRDC contains at least one compact (≤ 0.5 pc) core, with most IRDCs containing multiple cores.

IRDCs have masses in the range 120 to 16,000 $M_\odot$ (with a median mass of 940 $M_\odot$) and, in some cases, are associated with bright mid-IR emission sources. We suggest that the degree to which IRDCs are associated with bright mid-IR emission sources is related to their evolutionary phase; IRDCs with no associated mid-IR emission sources are in the earliest phase, while IRDCs with several bright mid-IR emission sources are in the later stages. The colder temperatures, fragmented sub-structure, and similar sizes and masses of IRDCs and cluster-forming molecular clumps, support our idea that IRDCs may be the precursors to cluster-forming molecular clumps and the high-mass analogs to Bok globules.

Toward the 38 IRDCs, we detected a total of 140 millimeter cores unassociated with *MSX* 8 μm emission. The core masses range from 10 to 2,100 $M_\odot$ and have a median mass of 120 $M_\odot$. We find that IRDC cores have similar sizes, masses, and densities to hot cores associated with individual high-mass stars, the only obvious difference being that IRDC cores are colder. Assuming typical star formation efficiencies ($\sim 20\%$), the simplest interpretation is that the majority of the cores will form high-mass stars in the range 6 to 60 $M_\odot$. We suggest therefore that IRDC cores are in an earlier evolutionary phase than hot cores and that they are the higher-mass analog to the pre-protostellar cores within Bok globules.

Given the limited angular resolution and sensitivity of the 1.2 mm continuum images, we cannot yet exclude the possibility that many of the cores will further fragment to form low- to intermediate-mass stars or that many low-mass cores exist within IRDCs but are below our detection limit. However, an estimate of the star formation rate within IRDC-like molecular clumps ($\sim 2\ M_\odot\,\mathrm{yr}^{-1}$) is comparable to the global star formation rate in the Galaxy, which supports the idea that such molecular clumps may be the birthplaces of all stars. We also find the slope of the IRDC core mass spectrum ($\alpha \sim 2.1 \pm 0.4$) is similar to that of the stellar IMF.

Future high-resolution studies of IRDCs may help solve several outstanding problems in cluster formation. For example, the location of cores of various masses within IRDCs will test the idea that the observed stellar mass segregation (the tendency for higher mass stars to be located nearer to the center of a cluster) in evolved clusters results from an earlier mass segregation of the proto-stellar cores (Gouliermis et al. 2004). In addition, emission from the extended regions of IRDCs will trace the initial conditions and cloud density structure just prior to fragmentation. IRDCs, therefore, represent excellent laboratories to study the core mass spectrum, its relation to the stellar initial mass function, and the observed mass segregation within star clusters.

The authors gratefully acknowledge funding support through NASA grant NNG04GGC92G. We thank Axel Weiss for help with the IRAM observations. The data have been reduced with the mapping software package developed by Robert Zylka. This software uses the "restoring" algorithm of Emerson et al. (1979), the "converting" algorithm of C. Salter ("Continuum Mapping with the NRAO 12-m Telescope" user's manual), and partly the NOD2 and the GILDAS libraries. IRAM is supported by INSU/CNRS (France), MPG (Germany) and IGN (Spain). This research made use of data products from the *Midcourse Space Experiment*. Processing of the data was funded by the Ballistic Missile Defense Organization with additional support from NASA Office of Space Science. This research has also made use of the NASA/IPAC Infrared Science Archive, which is operated by the Jet Propulsion Laboratory, California Institute of Technology, under contract with the National Aeronautics and Space Administration. We thank the anonymous referee for suggesting several clarifications and augmentations that have greatly improved the paper.

REFERENCES

Adams, F. C., Lada, C. J., & Shu, F. H. 1987, ApJ, 312, 788
Alves, J. F., Lada, C. J., & Lada, E. A. 2001, Nature, 409, 159
Bally, J., & Lada, C. J. 1983, ApJ, 265, 824
Benjamin, R. A., et al. 2003, PASP, 115, 953
Blitz, L. & Williams, J. P. 1999, in NATO ASIC Proc. 540: The Origin of Stars and Planetary Systems, 3
Bok, B. J., & Reilly, E. F. 1947, ApJ, 105, 255
Bourke, T. L., Hyland, A. R., & Robinson, G. 1995, MNRAS, 276, 1052
Brand, J., & Blitz, L. 1993, A&A, 275, 67
Carey, S. J., Clark, F. O., Egan, M. P., Price, S. D., Shipman, R. F., & Kuchar, T. A. 1998, ApJ, 508, 721
Carey, S. J., Feldman, P. A., Redman, R. O., Egan, M. P., MacLeod, J. M., & Price, S. D. 2000, ApJ, 543, L157
Churchwell, E. 2002, ARA&A, 40, 27
Clemens, D. P. 1985, ApJ, 295, 422
Clemens, D. P., & Barvainis, R. 1988, ApJS, 68, 257
Egan, M. P., Shipman, R. F., Price, S. D., Carey, S. J., Clark, F. O., & Cohen, M. 1998, ApJ, 494, L199
Emerson, D. T., Klein, U., & Haslam, C. G. T. 1979, A&A, 76, 92
Fukui, Y., Iwata, T., Mizuno, A., Bally, J., & Lane, A. P. 1993, Protostars and Planets III, 603
Garay, G., Faúndez, S., Mardones, D., Bronfman, L., Chini, R., & Nyman, L.-Å. 2004, ApJ, 610, 313
Garay, G. & Lizano, S. 1999, PASP, 111, 1049
Goldsmith, P. F. 1987, ASSL Vol. 134: Interstellar Processes, 51
Gouliermis, D., Keller, S. C., Kontizas, M., Kontizas, E., & Bellas-Velidis, I. 2004, A&A, 416, 137
Hennebelle, P., Pérault, M., Teyssier, D., & Ganesh, S. 2001, A&A, 365, 598
Hildebrand, R. H. 1983, QJRAS, 24, 267
Jackson, J. M., Rathborne, J. M., Shah, R. Y., Simon, R., Bania, T. M., Clemens, D. P., Chambers, E. T., Johnson, A. M., Dormody, M., Lavoie, R., & Heyer, M. 2006, ApJ, accepted
Kramer, C., Stutzki, J., Rohrig, R., & Corneliussen, U. 1998, A&A, 329, 249
Kurtz, S., Cesaroni, R., Churchwell, E., Hofner, P., & Walmsley, C. M. 2000, Protostars and Planets IV, 299
Lada, C. J., & Wilking, B. A. 1984, ApJ, 287, 610
Lada, C. J., Lada, E. A., Clemens, D. P., & Bally, J. 1994, ApJ, 429, 694
Lada, C. J. 1999, NATO ASIC Proc. 540: The Origin of Stars and Planetary Systems, 143
Lada, C. J. & Lada, E. A. 2003, ARA&A, 41, 57
Lada, E. A., Evans, N. J., & Falgarone, E. 1997, ApJ, 488, 286
Leung, C. M. 1985, Protostars and Planets II, 104
Lis, D. C. & Carlstrom, J. E. 1994, ApJ, 424, 189
Lombardi, M., & Alves, J. 2001, A&A, 377, 1023
Motte, F., Andre, P., & Neri, R. 1998, A&A, 336, 150
Motte, F., Schilke, P., & Lis, D. C. 2003, ApJ, 582, 277
Myers, P. C., & Benson, P. J. 1983, ApJ, 266, 309
Ormel, C. W., Shipman, R. F., Ossenkopf, V., & Helmich, F. P. 2005, A&A, 439, 613
Ossenkopf, V. & Henning, T. 1994, A&A, 291, 943
Perault, M., Omont, A., Simon, G., Seguin, P., Ojha, D., Blommaert, J., Felli, M., Gilmore, G., Guglielmo, F., Habing, H., Price, S., Robin, A., de Batz, B., Cesarsky, C., Elbaz, D., Epchtein, N., Fouque, P., Guest, S., Levine, D., Pollock, A., Prusti, T., Siebenmorgen, R., Testi, L., & Tiphene, D. 1996, A&A, 315, L165
Prantzos, N. & Aubert, O. 1995, A&A, 302, 69
Price, S. D., Egan, M. P., Carey, S. J., Mizuno, D., & Kuchar, T. 2001, AJ, 121, 2819
Rathborne, J. M., Jackson, J. M., Chambers, E. T., Simon, R., Shipman, R., & Frieswijk, W. 2005, ApJ, 630, L181
Redman, R. O., Feldman, P. A., Wyrowski, F., Côté, S., Carey, S. J., & Egan, M. P. 2003, ApJ, 586, 1127
Salpeter, E. E. 1955, ApJ, 121, 161
Shu, F. H., Adams, F. C., & Lizano, S. 1987, ARA&A, 25, 23
Shu, F. H. 1991, NATO ASIC Proc. 342: The Physics of Star Formation and Early Stellar Evolution, 365
Simon, R., Jackson, J. M., Clemens, D. P., Bania, T. M., & Heyer, M. H. 2001, ApJ, 551, 747
Simon, R., Jackson, J. M., Rathborne, J. M., & Chambers, E. T. 2006a, ApJ, accepted
Simon, R., Rathborne, J. M., Shah, R. Y., Jackson, J. M., & Chambers, E. T. 2006b, ApJ, submitted
Snell, R. L., Loren, R. B., & Plambeck, R. L. 1980, ApJ, 239, L17
Testi, L. & Sargent, A. I. 1998, ApJ, 508, L91
Teyssier, D., Hennebelle, P., & Pérault, M. 2002, A&A, 382, 624
van Dishoeck, E. F., & Hogerheijde, M. R. 1999, NATO ASIC Proc. 540: The Origin of Stars and Planetary Systems, 97
Ward-Thompson, D., Scott, P. F., Hills, R. E., & Andre, P. 1994, MNRAS, 268, 276
Williams, J. P., Blitz, L., & McKee, C. F. 2000, Protostars and Planets IV, 97

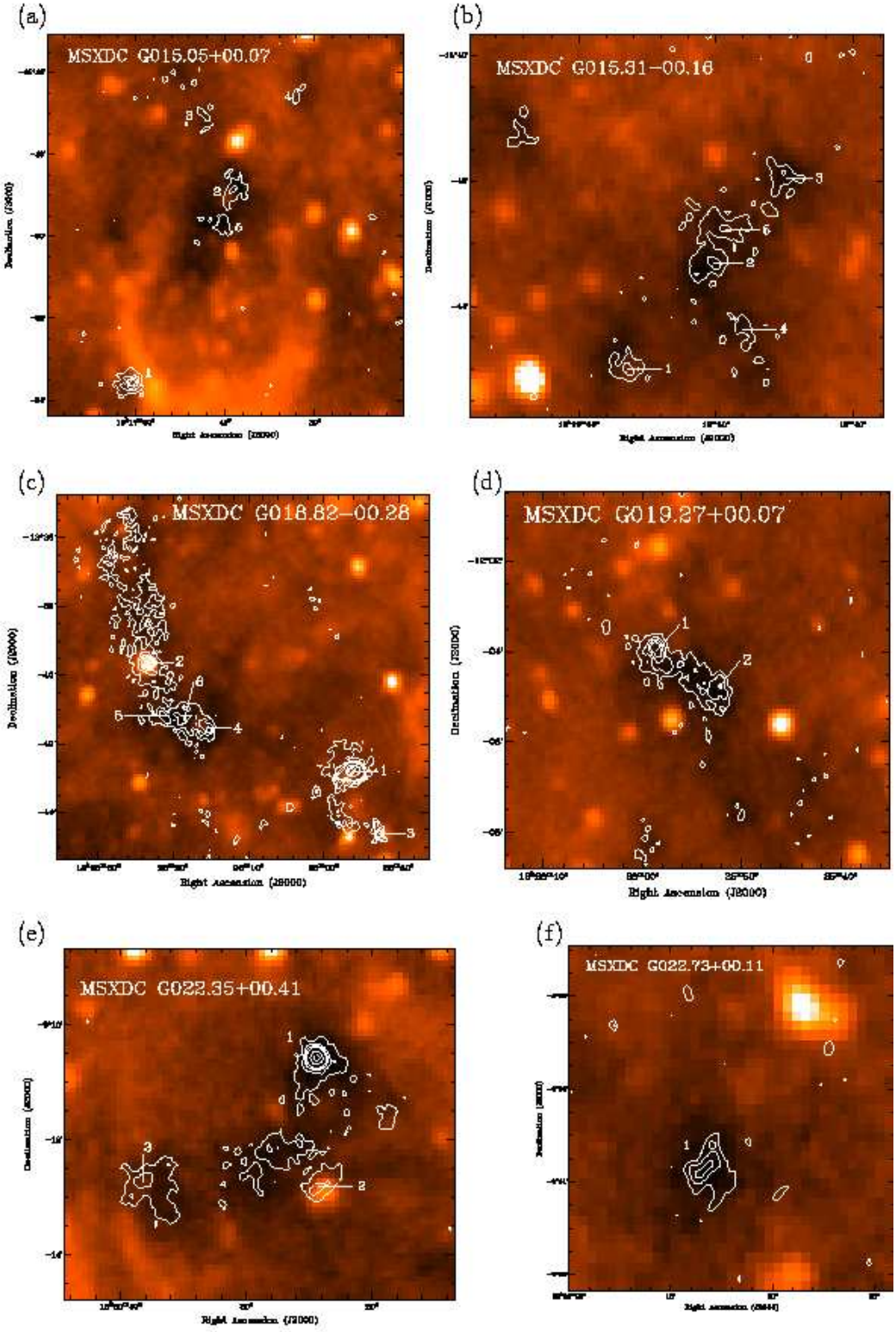

FIG. 1.— *MSX* 8 μm images overlaid with 1.2 mm continuum emission for six IRDCs. The 1.2 mm cores identified within the IRDCs are labeled with their designation (as listed in Table 3). The contours in all cases are 30 ($\sim 3\sigma$), 60, 90, 120, 240, 360, 480, 840, 1200, 2400 mJy beam^{-1}, except for G015.31−00.16 which has contours of 20 and 40 mJy beam $^{-1}$ and G022.73+00.11 which has contours of 20, 30, 45 mJy beam^{-1}.

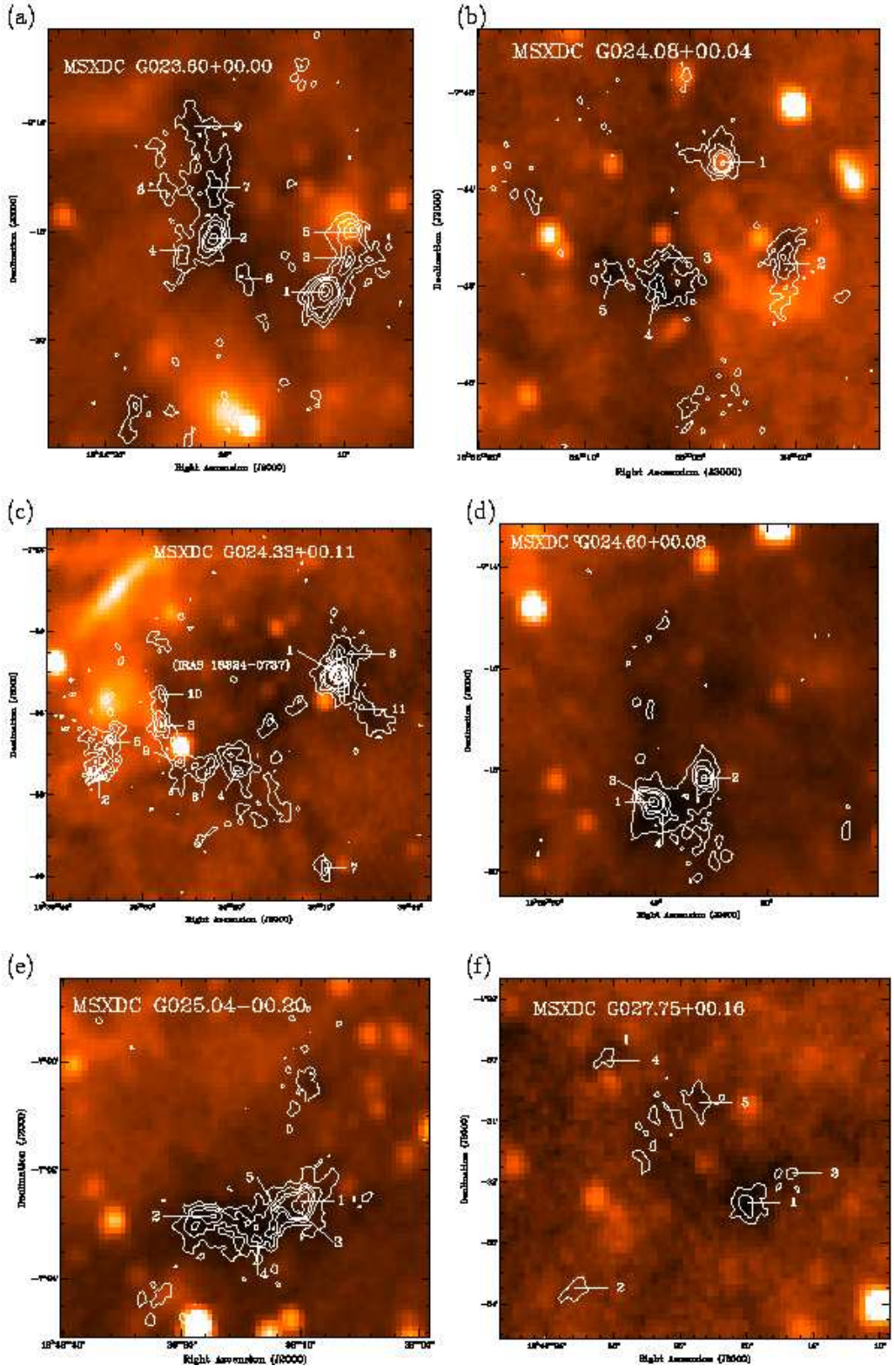

FIG. 2.— *MSX* 8 μm images overlaid with 1.2 mm continuum emission for six IRDCs. The 1.2 mm cores identified within the IRDCs are labeled with their designation (as listed in Table 3). The contours in all cases are 30 ($\sim 3\sigma$), 60, 90, 120, 240, 360, 480, 840, 1200, 2400 mJy beam^{-1}. The ellipse overlaid on G024.33+00.11 marks the position of the IRAS source.

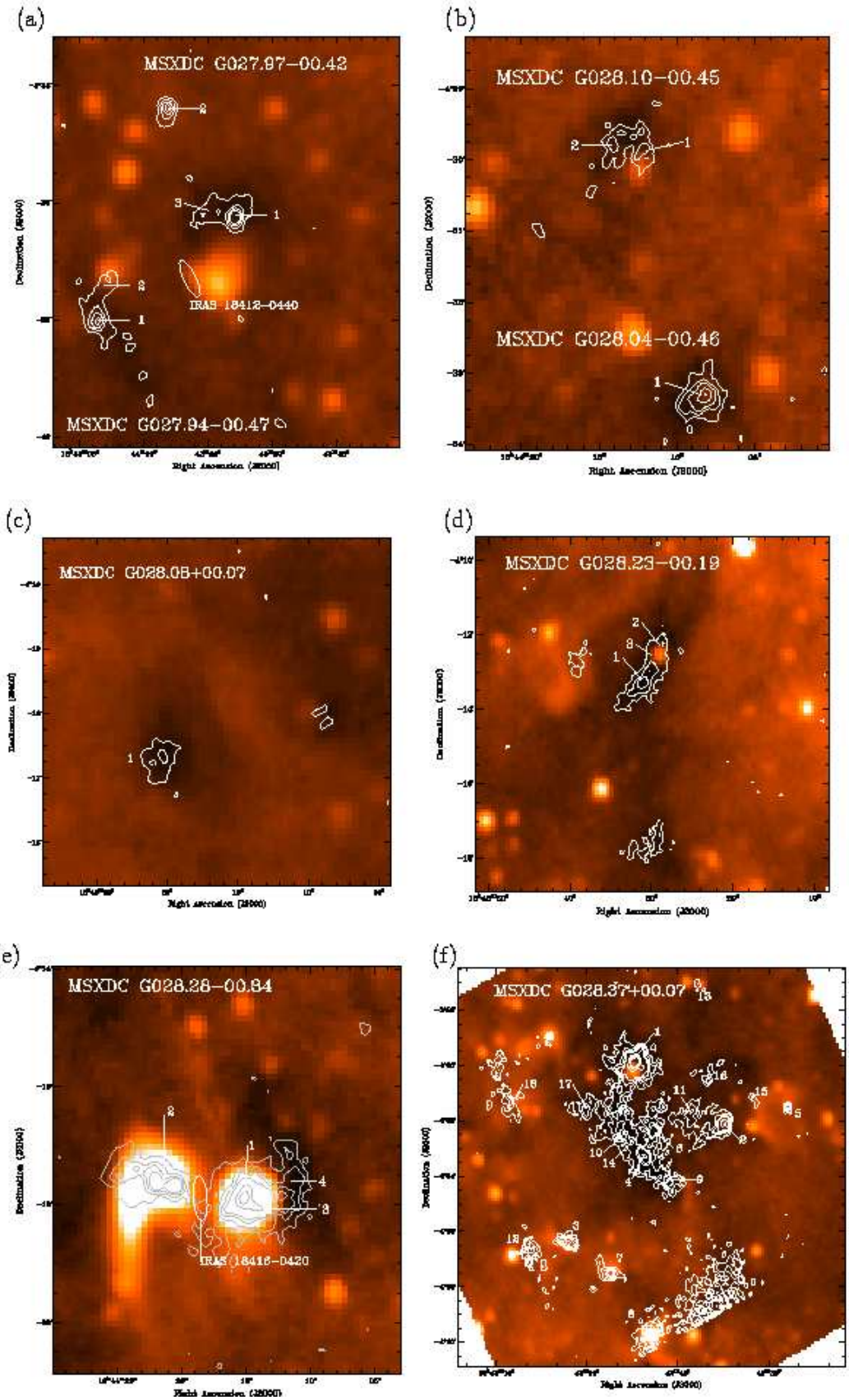

FIG. 3.— *MSX* 8 μm images overlaid with 1.2 mm continuum emission for six IRDCs. The 1.2 mm cores identified within the IRDCs are labeled with their designation (as listed in Table 3). The contours in all cases are 30 ($\sim 3\sigma$), 60, 90, 120, 240, 360, 480, 840, 1200, 2400 mJy beam^{-1}. The ellipses mark the position of the labeled IRAS sources.

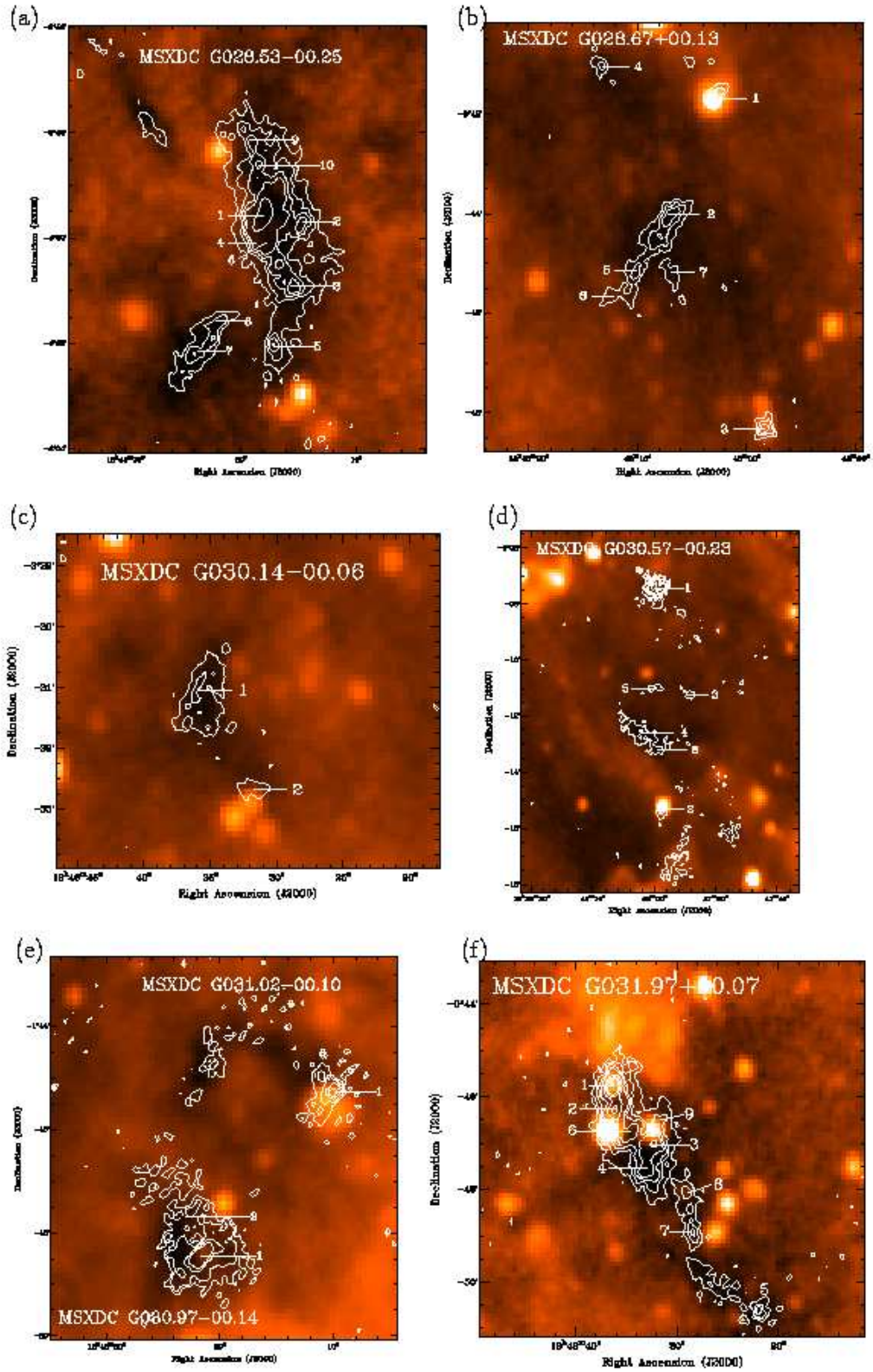

FIG. 4.— *MSX* 8 μm images overlaid with 1.2 mm continuum emission for six IRDCs. The 1.2 mm cores identified within the IRDCs are labeled with their designation (as listed in Table 3). The contours in all cases are 30 ($\sim 3\sigma$), 60, 90, 120, 240, 360, 480, 840, 1200, 2400 mJy beam^{-1}.

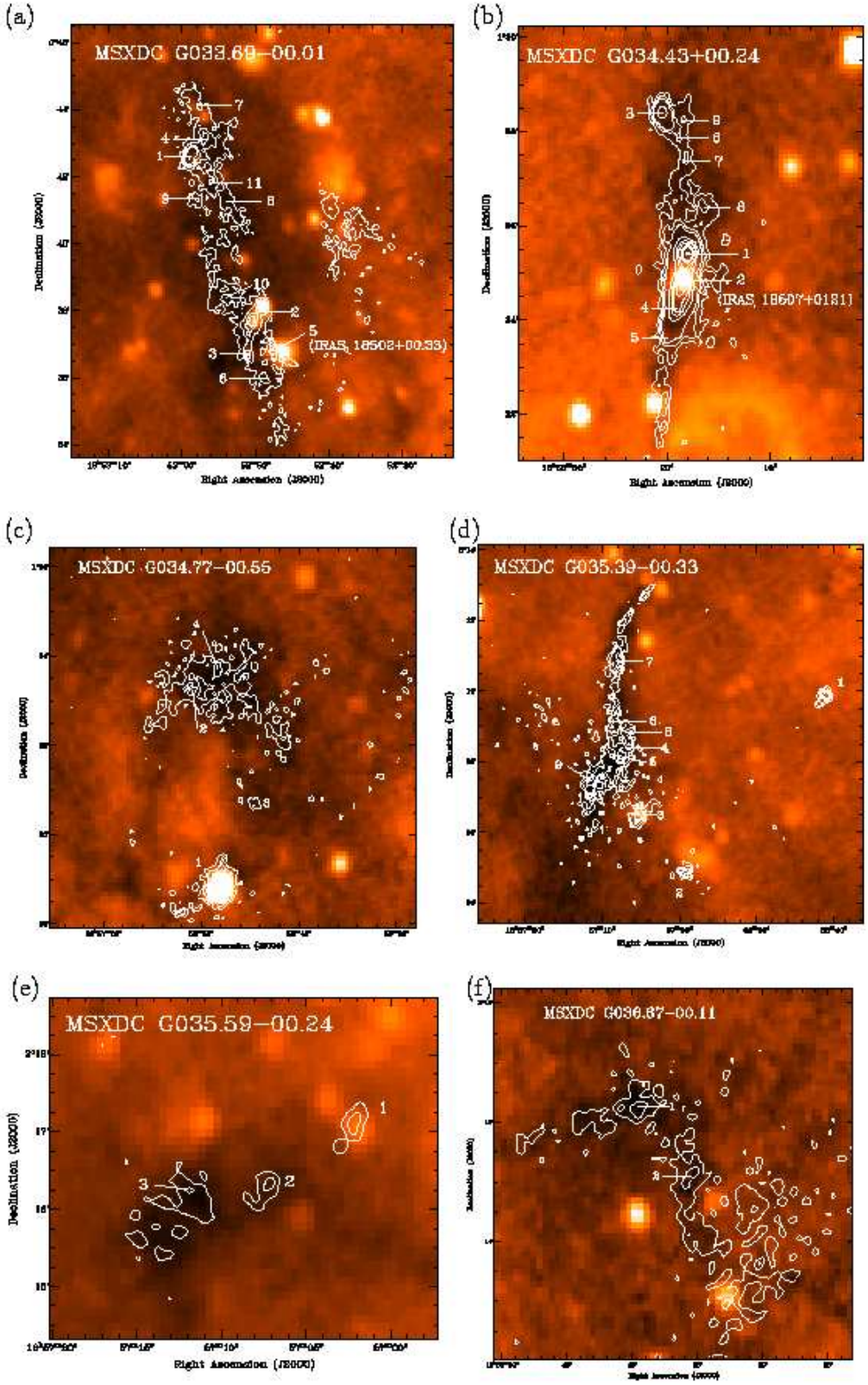

FIG. 5.— *MSX* 8 μm images overlaid with 1.2 mm continuum emission for six IRDCs. The 1.2 mm cores identified within the IRDCs are labeled with their designation (as listed in Table 3). The contours in all cases are 30 ($\sim 3\sigma$), 60, 90, 120, 240, 360, 480, 840, 1200, 2400 mJy beam^{-1}, except for G034.43+00.24 which starts at 60 mJy beam^{-1}. The ellipse marks the position of the IRAS source.

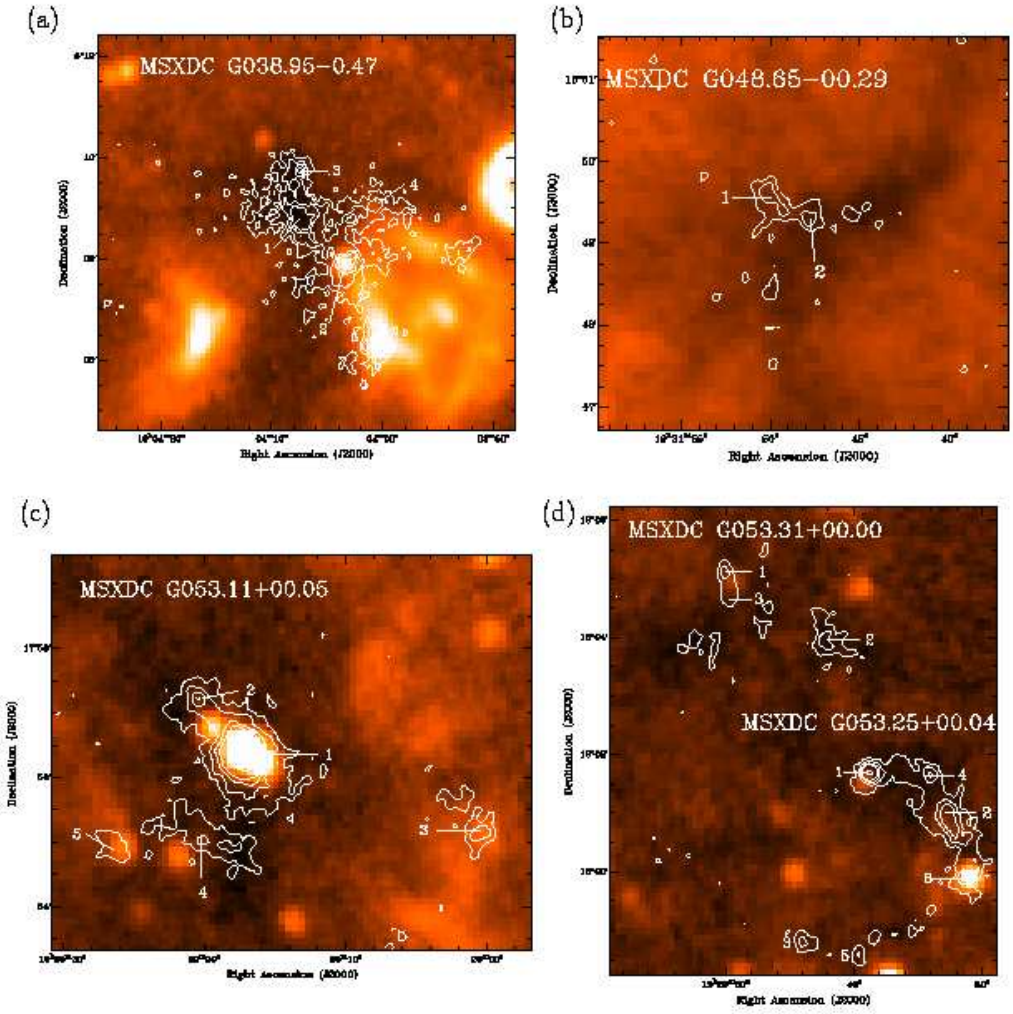

FIG. 6.— *MSX* 8 μm images overlaid with 1.2 mm continuum emission for six IRDCs. The 1.2 mm cores identified within the IRDCs are labeled with their designation (as listed in Table 3). The contours in all cases are 30 ($\sim 3\sigma$), 60, 90, 120, 240, 360, 480, 840, 1200, 2400 mJy beam^{-1}.

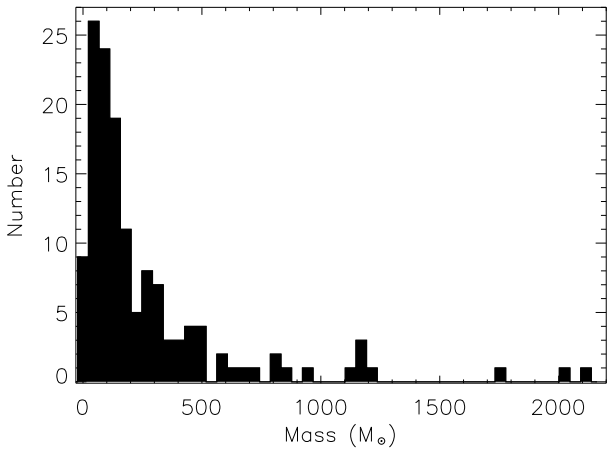

FIG. 7.— Number distribution of compact 1.2 mm cores with mass. We find the cores have masses in the range 10 to 2100 $M_\odot$ with a median mass of 120 $M_\odot$. A power law fit to the curve (above a mass of 100 $M_\odot$) gives a slope of 2.1±0.4. We find that ∼ 67% of our sample lies in the mass range 30 to 300 $M_\odot$. The apparent peak near M ∼45 $M_\odot$ reflects our detection limit.

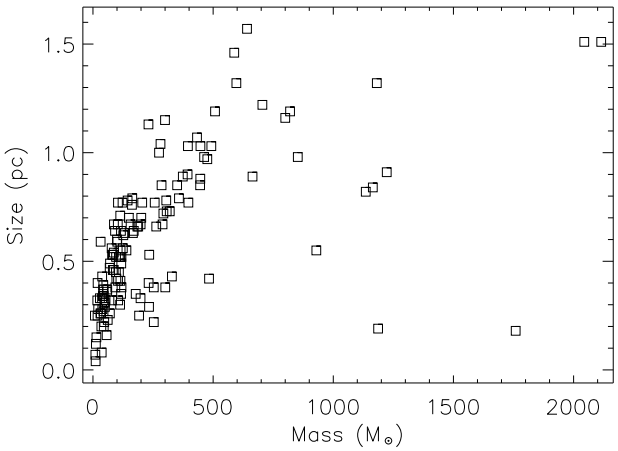

FIG. 8.— Size versus mass for the compact 1.2 mm cores. The cores have sizes in the range 0.04 to 1.6 pc, with a median value of 0.5 pc.

TABLE 1
COMPARISON OF MOLECULAR CLUMP AND CORE PROPERTIES

Properties	Bok globules	Cluster-forming clumps	IRDCs	Cores		
				pre-protostellar	Hot	IRDC
Radius (pc)	0.1–2	0.5–1	1–3	∼0.05	<0.1	0.02–0.8
Mass ($M_\odot$)	1–10^2	10^2–10^3	10^2–10^4	0.5–5	∼10^2	10–10^3
Density (cm^{-3})	10^3–10^4	10^4–10^7	10^2–10^4	10^5–10^6	10^5–10^8	10^3–10^7
Temperature (K)	10–20	50–200	10-20	10	50–250	15–30
References	1,2,3	4,5	6	7,8	9,10,11	12,13

References. — (1) Leung (1985); (2) Clemens & Barvainis (1988); (3) Bourke et al. (1995); (4) Lada & Lada (2003); (5) Motte et al. (2003); (6) this work; (7) Myers & Benson (1983); (8) Ward-Thompson et al. (1994); (9) Garay & Lizano (1999); (10) Kurtz et al. (2000); (11) Churchwell (2002); (12) this work; (13) Rathborne et al. (2005).

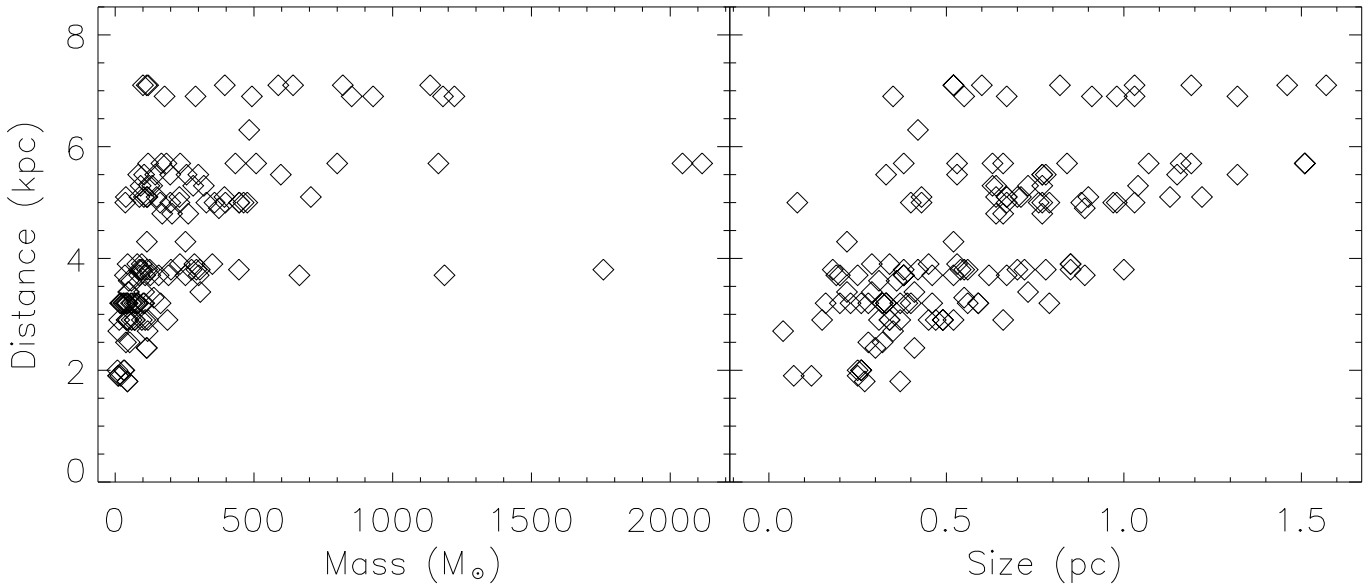

FIG. 9.— Distance as a function of 1.2 mm core mass (left) and size (right). We find no correlation between either mass or size and distance to the cores. Indeed, we detect low-mass cores at all distances.

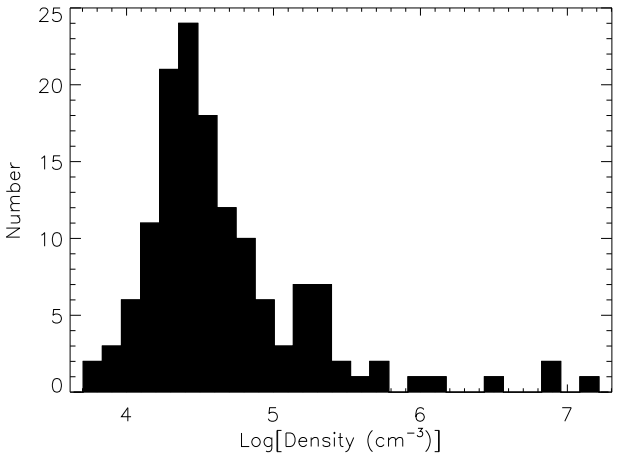

FIG. 10.— Number distribution of compact 1.2 mm cores with density. We find the densities range from 10^3 to 10^7 cm^{-3}, with a median value of 3.3×10^4 cm^{-3}.

TABLE 2
PROPERTIES OF THE IRDCS

Name	Coordinates		V_{LSR}	ΔV	D	1.2 mm Flux		Mass
	α	δ				Peak	Integrated	
MSXDC	(J2000)	(J2000)	($\mathrm{km\,s^{-1}}$)	($\mathrm{km\,s^{-1}}$)	(kpc)	(mJy)	(Jy)	$M_{\odot}$
G015.05+00.07	18 17 41.8	-15 49 38.7	30.9	6.8	3.2	115	0.71	158
G015.31−00.16	18 18 51.4	-15 43 27.7	31.1	3.3	3.2	41	1.67	370
G018.82−00.28	18 26 19.8	-12 41 29.7	65.8	5.5	4.8	80	6.36	3168
G019.27+00.07	18 25 54.0	-12 04 56.3	26.2	4.5	2.4	150	3.25	405
G022.35+00.41	18 30 24.7	-09 10 47.4	60.5	2.2	4.3	349	3.71	1483
G022.73+00.11	18 32 13.4	-09 00 58.5	77.8	7.0	5.1	38	0.72	405
G023.60+00.00	18 34 21.0	-08 17 31.1	53.9	5.8	3.9	272	8.83	2903
G024.08+00.04	18 35 02.9	-07 46 11.8	52.5	5.8	3.8	68	3.04	949
G024.33+00.11	18 35 16.3	-07 36 09.3	52.9	6.5	3.8	1199	8.34	2603
G024.60+00.08	18 35 39.4	-07 18 50.9	51.7	3.9	3.7	263	4.22	1249
G025.04−00.20	18 37 26.6	-07 09 14.2	46.9	4.2	3.4	92	6.07	1517
G027.75+00.16	18 41 20.4	-04 32 25.1	79.1	6.9	5.3	75	0.99	599
G027.94−00.47	18 44 01.5	-04 38 41.6	45.7	3.1	3.2	103	1.55	343
G027.97−00.42	18 43 52.8	-04 36 13.6	45.9	3.5	3.2	143	1.61	356
G028.04−00.46	18 44 10.3	-04 33 37.1	45.5	3.0	3.2	84	0.64	142
G028.08+00.07	18 42 20.4	-04 16 50.3	75.8	5.4	4.9	63	0.72	374
G028.10−00.45	18 44 13.6	-04 29 47.4	46.2	2.5	3.2	33	1.80	398
G028.23−00.19	18 43 31.3	-04 13 18.4	79.6	6.5	5.1	83	2.80	1574
G028.28−00.34	18 44 11.0	-04 17 39.2	47.4	4.5	3.3	64	6.19	1457
G028.37+00.07	18 42 50.6	-04 03 30.4	78.6	8.3	5.0	199	29.41	15895
G028.53−00.25	18 44 17.1	-03 59 36.6	87.0	4.7	5.7	227	15.96	11210
G028.67+00.13	18 43 07.9	-03 44 28.5	79.5	8.0	5.1	70	1.67	939
G030.14−00.06	18 46 36.4	-02 31 22.1	86.7	4.0	5.5	53	1.22	798
G030.57−00.23	18 48 02.0	-02 12 40.1	86.2	4.0	5.5	55	2.47	1615
G030.97−00.14	18 48 24.2	-01 48 24.7	78.8	6.1	5.1	27	5.08	2856
G031.02−00.10	18 48 22.2	-01 45 03.2	78.0	5.9	5.0	45	0.30	157
G031.97+00.07	18 49 33.7	-00 47 48.3	96.7	6.2	6.9	311	16.32	14797
G033.69−00.01	18 52 57.6	00 42 58.9	105.9	6.1	7.1	205	12.14	13230
G034.43+00.24	18 53 18.9	01 26 38.6	57.1	5.8	3.7	2228	36.88	10914
G034.77−00.55	18 56 48.8	01 23 21.0	43.5	5.0	2.9	59	4.85	882
G035.39−00.33	18 57 09.0	02 07 45.7	44.7	3.6	2.9	76	8.40	1527
G035.59−00.24	18 57 11.7	02 15 54.7	44.7	4.3	2.9	57	0.67	121
G036.67−00.11	18 58 40.4	03 16 17.7	54.4	3.6	3.6	61	3.92	1098
G038.95−00.47	19 04 08.3	05 08 49.3	41.6	3.1	2.7	119	11.37	1792
G048.65−00.29	19 21 45.3	13 49 21.7	34.0	2.8	2.5	71	6.79	917
G053.11+00.05	19 29 18.1	17 54 33.0	22.0	2.2	1.8	81	7.41	519
G053.25+00.04	19 29 37.5	18 01 23.5	23.9	2.1	1.9	96	4.36	340
G053.31+00.00	19 29 54.5	18 03 30.0	24.0	2.7	2.0	71	4.54	393
References	1	1	2	2	2			

References. — (1) Simon et al. 2006a; (2) Simon et al. 2006b

TABLE 3
PROPERTIES OF THE IRDC CORES

Core	Coordinates		1.2 mm Flux		FWHM Diameter		Mass	Comment[a]
	α (J2000)	δ (J2000)	Peak (mJy)	Integrated (Jy)	Angular ($''$)	Physical (pc)	($M_\odot$)	
MSXDC G015.05+00.07								
MM1	18 17 50.4	-15 53 38	115	0.47	24	0.32	105	
MM2	18 17 40.0	-15 48 55	50	0.37	32	0.46	83	(b)
MM3	18 17 42.4	-15 47 03	35	0.10	22	0.28	22	
MM4	18 17 32.0	-15 46 35	35	0.19	28	0.39	43	
MM5	18 17 40.2	-15 49 47	30	0.13	24	0.33	29	
MSXDC G015.31-00.16								
MM1	18 18 56.4	-15 45 00	41	0.17	24	0.33	38	
MM2	18 18 50.4	-15 43 19	39	0.46	40	0.59	101	
MM3	18 18 45.3	-15 41 58	37	0.74	52	0.79	164	
MM4	18 18 48.0	-15 44 22	23	0.08	24	0.32	18	
MM5	18 18 49.1	-15 42 47	21	0.14	40	0.59	32	
MSXDC G018.82-00.28								
MM1	18 25 56.1	-12 42 48	459	1.78	23	0.46	887	em
MM2	18 26 23.4	-12 39 37	170	0.49	20	0.37	242	em
MM3	18 25 52.6	-12 44 37	118	0.47	25	0.52	233	em
MM4	18 26 15.5	-12 41 32	80	0.53	31	0.66	263	
MM5	18 26 21.0	-12 41 11	55	0.34	30	0.64	170	
MM6	18 26 18.4	-12 41 15	45	0.41	35	0.77	205	
MSXDC G019.27+00.07								
MM1	18 25 58.5	-12 03 59	150	0.91	29	0.30	113	
MM2	18 25 52.6	-12 04 48	89	0.92	37	0.41	114	
MSXDC G022.35+00.41								
MM1	18 30 24.4	-09 10 34	349	0.63	16	0.22	253	(a)
MM2	18 30 24.2	-09 12 44	67	0.54	33	0.64	215	em
MM3	18 30 38.1	-09 12 44	53	0.29	28	0.52	114	
MSXDC G022.73+00.11								
MM1	18 32 13.0	-09 00 50	38	0.27	31	0.70	149	
MSXDC G023.60+00.00								
MM1	18 34 11.6	-08 19 06	375	1.11	20	0.31	365	em
MM2	18 34 21.1	-08 18 07	272	0.71	19	0.29	233	
MM3	18 34 10.0	-08 18 28	81	0.81	41	0.74	266	em
MM4	18 34 23.0	-08 18 21	68	1.07	47	0.85	350	
MM5	18 34 09.5	-08 18 00	65	0.30	26	0.43	98	em
MM6	18 34 18.2	-08 18 52	61	0.29	27	0.45	96	
MM7	18 34 21.1	-08 17 11	58	0.87	47	0.85	286	
MM8	18 34 24.9	-08 17 14	40	0.14	22	0.34	45	
MM9	18 34 22.5	-08 16 04	39	0.24	31	0.53	80	
MSXDC G024.08+00.04								
MM1	18 34 57.0	-7 43 26	219	0.63	20	0.29	196	em
MM2	18 34 51.1	-7 45 32	68	0.64	40	0.70	201	
MM3	18 35 2.2	-7 45 25	50	0.40	33	0.56	124	
MM4	18 35 2.6	-7 45 56	48	0.37	32	0.55	115	
MM5	18 35 7.4	-7 45 46	40	0.28	32	0.54	87	
MSXDC G024.33+00.11								
MM1	18 35 07.9	-07 35 04	1199	2.03	15	0.18	1759	IRAS 18324-0737
MM2	18 35 34.5	-07 37 28	117	0.39	25	0.40	123	em
MM3	18 35 27.9	-07 36 18	96	0.41	25	0.40	126	em
MM4	18 35 19.4	-07 37 17	90	1.43	48	0.85	446	
MM5	18 35 33.8	-07 36 42	79	0.62	34	0.58	192	em
MM6	18 35 07.7	-07 34 33	77	0.94	41	0.72	293	
MM7	18 35 09.8	-07 39 48	77	0.30	24	0.38	93	
MM8	18 35 23.4	-07 37 21	72	0.98	44	0.78	305	
MM9	18 35 26.5	-07 36 56	66	0.88	46	0.82	273	em
MM10	18 35 27.9	-07 35 32	64	0.31	26	0.42	97	
MM11	18 35 05.1	-07 35 58	48	0.88	56	1.00	275	
MSXDC G024.60+00.08								
MM1	18 35 40.2	-07 18 37	279	0.65	18	0.25	192	
MM2	18 35 35.7	-07 18 09	230	0.53	18	0.42	483	
MM3	18 35 41.1	-07 18 30	71	0.12	16	0.20	35	
MM4	18 35 39.3	-07 18 51	30	0.09	23	0.36	27	
MSXDC G025.04-00.20								
MM1	18 38 10.2	-07 02 34	203	1.11	28	0.42	276	em
MM2	18 38 17.7	-07 02 51	92	0.42	28	0.41	104	
MM3	18 38 10.2	-07 02 44	90	0.19	18	0.22	47	
MM4	18 38 13.7	-07 03 12	82	1.23	46	0.73	307	
MM5	18 38 12.0	-07 02 44	73	0.20	21	0.29	50	
MSXDC G027.75+00.16								
MM1	18 41 19.9	-04 32 20	75	0.53	31	0.73	320	(a)
MM2	18 41 33.0	-04 33 44	46	0.22	27	0.63	133	
MM3	18 41 16.8	-04 31 55	36	0.46	42	1.04	281	
MM4	18 41 30.4	-04 30 00	29	0.20	32	0.77	123	
MM5	18 41 23.6	-04 30 42	28	0.15	28	0.64	92	
MSXDC G027.94-00.47								
MM1	18 44 03.6	-04 38 00	103	0.32	21	0.26	70	
MM2	18 44 03.1	-04 37 25	40	0.19	27	0.37	42	
MSXDC G027.97-00.42								
MM1	18 43 52.8	-04 36 13	143	0.26	16	0.16	57	(a)
MM2	18 43 58.0	-04 34 24	103	0.28	19	0.23	62	(b)

TABLE 3—*Continued*

Core	Coordinates		1.2 mm Flux		FWHM Diameter		Mass	Comment[a]
	α (J2000)	δ (J2000)	Peak (mJy)	Integrated (Jy)	Angular ($''$)	Physical (pc)	($M_\odot$)	
MM3	18 43 54.9	-04 36 08	41	0.27	18	0.20	45	
MSXDC G028.04-00.46								
MM1	18 44 08.5	-04 33 22	87	0.36	24	0.32	80	em
MSXDC G028.08+00.07								
MM1	18 42 20.3	-04 16 42	63	0.72	39	0.89	374	
MSXDC G028.10-00.45								
MM1	18 44 12.9	-04 29 45	33	0.35	38	0.56	78	
MM2	18 44 14.3	-04 29 48	18	0.09	28	0.40	19	
MSXDC G028.23-00.19								
MM1	18 43 30.7	-04 13 12	83	1.25	51	1.22	705	(a)
MM2	18 43 29.0	-04 12 16	35	0.19	27	0.60	108	em
MM3	18 43 30.0	-04 12 33	23	0.07	21	0.43	38	
MSXDC G028.28-00.34								
MM1	18 44 15.0	-04 17 54	317	1.74	27	0.39	411	em
MM2	18 44 21.3	-04 17 37	165	1.36	37	0.55	321	em
MM3	18 44 13.4	-04 18 05	139	0.29	17	0.20	68	em
MM4	18 44 11.4	-04 17 22	64	0.59	37	0.55	139	
MSXDC G028.37+00.07								
MM1	18 42 52.1	-03 59 45	470	2.12	26	0.55	1148	em
MM2	18 42 37.6	-04 02 05	277	1.00	22	0.46	542	em
MM3	18 43 03.1	-04 06 24	248	0.89	23	0.47	482	em
MM4	18 42 50.7	-04 03 15	199	0.61	21	0.43	329	
MM5	18 42 26.8	-04 01 30	151	0.33	17	0.30	177	em
MM6	18 42 49.0	-04 02 23	145	0.43	20	0.40	232	
MM7	18 42 56.3	-04 07 31	138	0.56	24	0.51	304	em
MM8	18 42 49.7	-04 09 54	115	0.77	31	0.70	414	em
MM9	18 42 46.7	-04 04 08	97	0.73	34	0.77	397	
MM10	18 42 54.0	-04 02 30	88	0.66	34	0.79	358	
MM11	18 42 42.7	-04 01 44	81	0.83	38	0.88	447	
MM12	18 43 09.9	-04 06 52	71	0.88	42	0.97	476	
MM13	18 42 41.8	-03 57 08	66	0.86	42	0.98	463	
MM14	18 42 52.6	-04 02 44	62	0.07	12	0.08	36	
MM15	18 42 32.4	-04 01 16	59	0.25	26	0.55	134	em
MM16	18 42 40.2	-04 00 23	58	0.83	44	1.03	447	
MM17	18 43 00.0	-04 01 34	56	0.37	30	0.67	198	
MM18	18 43 12.9	-04 01 16	54	0.30	34	0.76	162	
MSXDC G028.53-00.25								
MM1	18 44 18.0	-03 59 34	227	1.66	33	0.84	1165	(a)
MM2	18 44 15.7	-03 59 41	129	3.01	56	1.51	2115	
MM3	18 44 16.0	-04 00 48	126	2.91	56	1.51	2044	
MM4	18 44 18.6	-04 00 05	95	1.14	44	1.16	800	
MM5	18 44 17.0	-04 02 04	95	0.33	23	0.53	234	
MM6	18 44 17.8	-04 00 05	71	0.17	18	0.38	119	
MM7	18 44 23.7	-04 02 09	63	0.72	45	1.19	508	(b)
MM8	18 44 22.0	-04 01 35	61	0.26	27	0.66	185	
MM9	18 44 19.3	-03 58 05	58	0.24	26	0.63	166	
MM10	18 44 18.5	-03 58 43	57	0.62	41	1.07	433	
MSXDC G028.67+00.13								
MM1	18 43 03.1	-03 41 41	86	0.25	20	0.40	143	em
MM2	18 43 07.1	-03 44 01	70	0.70	38	0.90	394	
MM3	18 42 58.2	-03 48 20	60	0.22	22	0.46	122	em
MM4	18 43 13.2	-03 41 03	37	0.21	29	0.64	116	
MM5	18 43 10.1	-03 45 08	32	0.18	30	0.67	103	
MM6	18 43 12.2	-03 45 39	31	0.20	31	0.71	113	
MM7	18 43 06.9	-03 45 11	27	0.16	30	0.67	87	
MSXDC G030.14-00.06								
MM1	18 46 35.7	-02 31 03	53	0.90	51	1.32	597	
MM2	18 46 31.7	-02 32 41	36	0.13	23	0.53	83	
MSXDC G030.57-00.23								
MM1	18 48 00.0	-02 07 20	297	0.60	17	0.33	419	em
MM2	18 47 58.7	-02 15 20	143	0.30	17	0.33	198	em
MM3	18 47 54.5	-02 11 15	55	0.39	31	0.77	257	
MM4	18 48 01.8	-02 12 35	37	0.46	45	1.15	300	(a)
MM5	18 47 59.9	-02 11 01	36	0.22	32	0.78	144	
MM6	18 47 59.4	-02 13 13	33	0.16	31	0.77	104	
MSXDC G030.97-00.14								
MM1	18 48 21.6	-01 48 27	114	0.74	32	0.73	417	em
MM2	18 48 22.0	-01 47 42	27	0.41	47	1.13	231	
MSXDC G031.02-00.10								
MM1	18 48 20.7	-01 44 48	130	0.65	24	0.50	349	em
MSXDC G031.97+00.07								
MM1	18 49 36.3	-00 45 45	913	1.84	17	0.40	1890	em; IRAS 18470-0049
MM2	18 49 36.0	-00 46 16	311	0.90	20	0.55	929	
MM3	18 49 32.3	-00 47 02	187	1.19	30	0.91	1222	
MM4	18 49 33.0	-00 47 33	117	0.83	32	0.98	852	
MM5	18 49 21.9	-00 50 35	96	0.17	16	0.35	178	(b)
MM6	18 49 35.0	-00 46 44	96	1.15	41	1.32	1181	
MM7	18 49 28.4	-00 48 54	80	0.28	23	0.67	291	
MM8	18 49 29.1	-00 48 12	64	0.48	33	1.03	493	

TABLE 3—*Continued*

Core	Coordinates		1.2 mm Flux		FWHM Diameter		Mass	Comment[a]
	α (J2000)	δ (J2000)	Peak (mJy)	Integrated (Jy)	Angular ($''$)	Physical (pc)	($M_\odot$)	
MM9	18 49 31.6	-00 46 30	47	0.15	21	0.57	151	em
MSXDC G033.69-00.01								
MM1	18 52 58.8	00 42 37	205	1.04	27	0.82	1135	
MM2	18 52 49.9	00 37 57	115	1.23	42	1.37	1342	em
MM3	18 52 50.8	00 36 43	81	0.26	22	0.63	288	em
MM4	18 52 56.4	00 43 08	78	0.75	37	1.19	820	
MM5	18 52 47.8	00 36 47	56	0.22	24	0.73	243	em; IRAS 18502+00.33
MM6	18 52 48.7	00 35 58	47	0.36	32	1.03	395	
MM7	18 52 58.1	00 44 08	43	0.59	47	1.57	641	
MM8	18 52 53.9	00 41 16	41	0.54	44	1.46	588	
MM9	18 52 58.1	00 41 20	40	0.11	19	0.52	119	
MM10	18 52 52.7	00 38 35	40	0.10	19	0.52	114	
MM11	18 52 56.2	00 41 48	31	0.09	21	0.60	100	
MSXDC G034.43+00.24								
MM1	18 53 18.0	01 25 24	2228	4.01	16	0.19	1187	
MM2	18 53 18.6	01 24 40	964	4.33	26	0.42	1284	em; IRAS 18507+0121
MM3	18 53 20.4	01 28 23	244	1.02	24	0.38	301	
MM4	18 53 19.0	01 24 08	221	0.86	24	0.38	253	
MM5	18 53 19.8	01 23 30	122	2.24	51	0.89	664	
MM6	18 53 18.6	01 27 48	57	0.43	37	0.62	126	
MM7	18 53 18.3	01 27 13	55	0.29	28	0.46	87	
MM8	18 53 16.4	01 26 20	51	0.36	31	0.52	108	
MM9	18 53 18.4	01 28 14	50	0.53	39	0.67	157	
MSXDC G034.77-00.55								
MM1	18 56 48.2	01 18 47	232	0.91	23	0.28	166	em
MM2	18 56 50.3	01 23 16	59	1.04	49	0.66	188	
MM3	18 56 44.7	01 20 42	44	0.08	16	0.15	14	
MM4	18 56 48.9	01 23 34	42	0.38	36	0.47	70	
MSXDC G035.39-00.33								
MM1	18 56 41.2	02 09 52	128	0.42	21	0.25	76	em
MM2	18 56 59.2	02 04 53	114	0.25	17	0.18	45	em
MM3	18 57 05.3	02 06 29	107	0.44	24	0.30	79	em
MM4	18 57 06.7	02 08 23	76	0.59	34	0.45	108	
MM5	18 57 08.8	02 08 09	69	0.65	37	0.49	118	
MM6	18 57 08.4	02 09 09	56	0.39	37	0.49	71	
MM7	18 57 08.1	02 10 50	55	0.53	39	0.52	96	(c)
MM8	18 57 07.0	02 08 54	52	0.33	29	0.37	59	
MM9	18 57 11.2	02 07 27	50	0.23	27	0.34	42	
MSXDC G035.59-00.24								
MM1	18 57 02.3	02 17 04	69	0.36	28	0.36	65	em
MM2	18 57 07.4	02 16 14	57	0.26	25	0.31	48	
MM3	18 57 11.6	02 16 08	44	0.23	27	0.34	41	
MSXDC G036.67-00.11								
MM1	18 58 39.6	03 16 16	61	0.17	21	0.31	49	(a)
MM2	18 58 35.6	03 15 06	54	0.21	24	0.36	58	
MSXDC G038.95-0.47								
MM1	19 04 07.4	05 08 48	119	0.74	29	0.35	117	(a)
MM2	19 04 03.4	05 07 56	103	0.46	25	0.28	73	em
MM3	19 04 07.4	05 09 44	65	0.07	12	0.04	11	
MM4	19 04 00.6	05 09 06	53	0.31	33	0.40	48	em
MSXDC G048.65-00.29								
MM1	19 21 49.7	13 49 30	71	0.39	29	0.32	52	
MM2	19 21 47.6	13 49 22	57	0.29	26	0.28	39	
MSXDC G053.11+00.05								
MM1	19 29 17.2	17 56 21	536	1.77	21	0.15	124	em
MM2	19 29 20.2	17 57 06	81	0.63	33	0.27	44	
MM3	19 29 00.6	17 55 11	70	0.18	19	0.13	12	em
MM4	19 29 20.4	17 55 04	52	0.64	44	0.37	45	
MM5	19 29 26.3	17 54 53	48	0.19	24	0.18	13	em
MSXDC G053.25+00.04								
MM1	19 29 39.0	18 01 42	246	0.31	13	0.06	24	em
MM2	19 29 33.0	18 01 00	97	0.95	38	0.33	74	em
MM3	19 29 44.0	17 58 47	96	0.13	14	0.07	10	
MM4	19 29 34.5	18 01 39	71	0.15	17	0.12	12	
MM5	19 29 39.4	17 58 40	52	0.25	30	0.25	19	
MM6	19 29 31.5	17 59 50	47	0.22	26	0.21	17	em
MSXDC G053.31+00.00								
MM1	19 29 50.0	18 05 07	71	0.36	29	0.26	31	
MM2	19 29 42.1	18 03 57	60	0.38	30	0.26	33	
MM3	19 29 49.7	18 04 39	21	0.09	29	0.25	8	

[a]Includes: "em" marks cores that are associated with 8 μm emission in the *MSX* images; letters in parentheses refer to the corresponding cores from the IRDC catalog of Simon et al. (2006a); the names of IRAS sources associated with the millimeter cores are also listed here.